

A PARALLEL IMPLEMENTATION OF A DIAGONALIZATION-BASED PARALLEL-IN-TIME INTEGRATOR*

GAYATRI ČAKLOVIĆ ^{†‡}, ROBERT SPECK[†], AND MARTIN FRANK[‡]

Abstract. We present and analyze a parallel implementation of a parallel-in-time method based on α -circulant preconditioned Richardson iterations. While there are a lot of papers exploring this new class of single-level, time-parallel integrators from many perspectives, performance results of actual parallel runs are still missing. This leaves a critical gap, because the efficiency and applicability heavily rely on the actual parallel performance, with only limited guidance from theoretical considerations. Also, many challenges like selecting good parameters, finding suitable communication strategies, and performing a fair comparison to sequential time-stepping methods can be easily missed. In this paper, we first extend the original idea by using a collocation method of arbitrary order, which adds another level of parallelization in time. We derive an adaptive strategy to select a new α -circulant preconditioner for each iteration during runtime for balancing convergence rates, round-off errors and inexactness in the individual time-steps. After addressing these more theoretical challenges, we present an open-source space- and doubly-time-parallel implementation and evaluate its performance for two different test problems.

Key words. parallel-in-time integration, iterative methods, diagonalization, collocation, high-performance computing, petsc4py

AMS subject classifications. 65G50, 65M22, 65F10, 65Y05, 65Y20, 65M70

1. Introduction. Many flavors of numerical methods for computing the solution to an initial value problem exist. Usually, this is achieved in a sequential way, in the sense that an approximation of the solution at time-step comes from propagating an approximation at an earlier point in time with some numerical method that depends on the time-step size. Nowadays, parallelization of these algorithms in the temporal domain is gaining more and more attention due to growing number of available resources, parallel hardware and, recently, more and more mathematical approaches. First theories and proposals of parallelizing this process emerged in the 60s [27] and got real attention after the *Parareal* paper was published in 2001 [20]. As one of the key ideas, Parareal introduced coarsening in time to reduce the impact of the sequential nature of time stepping.

Parallel-in-Time (PinT) methods have been shown to be useful for quite a range of applications and we refer to the recent overview in [29] for more details. The research area is full of new ideas¹, with many covered in the seminal work '50 Years of Time Parallel Time Integration' [11]. However, while the theoretical analysis is rather advanced, only a few actual, parallel implementations on modern high-performance computing systems exist. Notable exceptions are the implementations of multigrid reduction in time [10, 24, 17], the parallel full approximation scheme in space and time [9, 23, 34], and the revisionist integral deferred correction method [28].

More often than not, expected and unexpected pitfalls occur when numerical methods are finally moved from a theoretical concept to an actual implementation, let alone on parallel machines. A sole convergence analysis of a method is often not enough to prove usefulness in terms of parallel scaling or reduced time-to-solution [16]. For example, mathematical theory has shown that the Parareal algorithm (as many

*Submitted to the editors on December 24, 2024.

[†]Jülich Supercomputing Centre, Forschungszentrum Jülich, Germany.

[‡]Department of Mathematics, Karlsruhe Institute of Technology, Germany

¹<https://parallel-in-time.org/references/>

others parallel-in-time methods) is either unstable or inefficient when applied to hyperbolic problems [35, 14, 36], therefore new ways to enhance it were developed [5, 13, 31]. Yet, most of these new approaches have more overhead, leading to less efficiency and applicability. One of many potential reasons is a phase-shift error arising from mismatches between the phase speed of coarse and fine propagator [30].

As an alternative, there exist methods such as paraexp [12] and REXI [19] which do not require coarsening in time altogether. Another parallel-in-time approach, which can be used without the need to coarsen, are iterative methods based on α -circulant preconditioners for “all-at-once” systems of partial differential equations (PDEs). This particular preconditioner is diagonalizable, resulting in decoupled systems across the time-steps, and early results indicate that these methods will also work for hyperbolic problems. It can be applied as preconditioners to GMRES or MINRES solvers [25, 26, 22] while other variants can be seen as a special versions of Parareal [15] or simple preconditioned Richardson iterations [39]. While many of these approaches show very promising results from a theoretical point of view, their efficient parallel implementations are often not demonstrated, not straightforward and, potentially, not possible. Selecting parameters, finding efficient communication strategies, and performing fair comparisons to sequential methods [16] are only three of many challenges in this regard.

The aim of this paper is to close this important gap for the class of α -circulant preconditioners, which is gaining more and more attention in the field of PinT. Using the preconditioned Richardson iteration with an α -circulant preconditioner as presented in [39], we describe the path from theory to implementation for these methods. We extend the original approach by using a collocation method as our base integrator and show that this choice not only yields time integrators of arbitrary order but also adds yet another level of parallelization in time. Following the taxonomy in [3], this yields a doubly-time parallel method, combining parallelization across the steps and parallelization across the method first proposed in [33]. We present and analyze an adaptive strategy to select the a new parameter α for each iteration in order to balance convergence rate of the method, round-off errors arising from the diagonalization of the preconditioner, and inexact system solves of the decoupled systems as the individual time-steps. After these more theoretical aspects, which, though, are crucial for an actual implementation, we present scaling results at the ‘sweet spot’ of two test problems: here, spatial and temporal errors are balanced and the speedup we measure on the parallel machine is the actual gain these methods can provide over the default sequential methods. These parallel runs represent a close enough picture for any application and variant using the diagonalization technique, narrowing the gap between real-life applications and theory. The code is freely available on GitHub [37], containing a short tutorial and all necessary scripts to reproduce the results presented here.

2. The method. In this section we briefly explain the derivation of our base numerical propagator: the collocation problem. After that, the formulation of the composite collocation problem on multiple steps is written down together with the preconditioned Richardson iteration which we use to solve this system parallel-in-time.

We focus on a linear initial value problem with an existing solution on some interval $[0, T]$, generally written as

$$(2.1) \quad u_t = \mathbf{A}u + b, \quad u(0) = u_0,$$

where $\mathbf{A} \in \mathbb{C}^{N \times N}$, $b : \mathbb{R} \rightarrow \mathbb{C}^N$ and $u_0 \in \mathbb{C}^N$, $N \in \mathbb{N}$. Let $0 = T_0 < T_1 < \dots < T_L =$

T be an equidistant subdivision of the time interval $[0, T]$ with a constant step size ΔT .

2.1. The composite collocation problem. Let $0 < t_1 < t_2 < \dots < t_M \leq \Delta T$ be a subdivision of $[0, \Delta T]$ using $M \in \mathbb{N}$ quadrature nodes and assume for simplicity $\Delta T = 1$. Under the assumption that $u \in \mathbb{C}^1([0, 1])$, an integral formulation in these nodes is given as

$$(2.2) \quad u(t_m) = u(0) + \int_0^{t_m} (\mathbf{A}u(s) + b(s))ds, \quad m = 1, \dots, M.$$

Approximating the subintegral function as a polynomial in the nodes yields

$$(2.3) \quad \int_0^{t_m} (\mathbf{A}u(s) + b(s))ds \approx \sum_{i=1}^M \left(\int_0^{t_m} c_i(s)ds \right) (\mathbf{A}u(t_i) + b(t_i)),$$

where c_i denotes the i th Lagrange polynomial, $i = 1, \dots, M$. Because of the integral approximation (2.3), the integral equation (2.2) can be rewritten in a matrix formulation known as the *collocation problem*:

$$(2.4) \quad (\mathbf{I}_{NM} - \mathbf{Q} \otimes \mathbf{A})\mathbf{u} = \mathbf{u}_0 + (\mathbf{Q} \otimes \mathbf{I}_N)\mathbf{b},$$

where $\mathbf{Q} \in \mathbb{R}^{M \times M}$ is a matrix with entries $q_{mi} = \int_0^{t_m} c_i(s)ds$, $\mathbf{u} = (u_1, \dots, u_M) \in \mathbb{C}^{MN}$ is the approximation of the solution u in t_m , $\mathbf{u}_0 = (u_0, \dots, u_0) \in \mathbb{C}^{MN}$, and $\mathbf{b} = (b_1, \dots, b_M) \in \mathbb{C}^{MN}$ is a vector of the function b evaluated in the quadrature nodes t_m . Generally, if one wants to solve the initial value problem on an interval of length ΔT , the matrix \mathbf{Q} in (2.4) is replaced with $\Delta T \mathbf{Q}$ which is verified by the corresponding change of variables in the integral. From now on, this notation will be used.

The collocation problem has been well-studied before [18]. For this work we will use Gauss-Radau quadrature nodes with the right node included. Then, $\|u(t_M) - u_M\| = O(\delta t^{2M-1})$, where $\delta t = \max_m(t_{m+1} - t_m)$ [2].

Define $\mathbf{C}_{\text{coll}} := \mathbf{I}_{MN} - \Delta T \mathbf{Q} \otimes \mathbf{A} \in \mathbb{C}^{MN \times MN}$ and let $\mathbf{H} := \mathbf{H}_M \otimes \mathbf{I}_N$, where $\mathbf{H}_M \in \mathbb{R}^{M \times M}$ denotes a matrix with zeros everywhere except ones in the last column. A discretized solution of (2.1) for L time-step on $[0, T]$ is obtained by solving

$$\begin{bmatrix} \mathbf{C}_{\text{coll}} & & & \\ -\mathbf{H} & \mathbf{C}_{\text{coll}} & & \\ & \ddots & \ddots & & \\ & & -\mathbf{H} & \mathbf{C}_{\text{coll}} & \\ & & & & \end{bmatrix} \begin{bmatrix} \mathbf{u}_1 \\ \mathbf{u}_2 \\ \vdots \\ \mathbf{u}_L \end{bmatrix} = \begin{bmatrix} \mathbf{u}_0 + \mathbf{v}_1 \\ \mathbf{v}_2 \\ \vdots \\ \mathbf{v}_L \end{bmatrix}$$

Here, the vectors $\mathbf{u}_l \in \mathbb{C}^{MN}$ represent the solution on $[T_l, T_{l+1}]$ and $\mathbf{v}_l = \Delta T(\mathbf{Q} \otimes \mathbf{I}_N)\mathbf{b}_l$, where \mathbf{b}_l is the function b evaluated in the corresponding quadrature nodes $T_l + t_1 < T_l + t_2 < \dots < T_l + t_M = T_{l+1}$ for that interval. More compactly, this can be written as

$$(2.5) \quad \mathbf{C}\vec{\mathbf{u}} := (\mathbf{I}_{LMN} - \mathbf{I}_L \otimes \mathbf{C}_{\text{coll}} + \mathbf{E} \otimes \mathbf{H})\vec{\mathbf{u}} = \vec{\mathbf{w}}$$

with $\vec{\mathbf{u}} = (\mathbf{u}_1, \mathbf{u}_2, \dots, \mathbf{u}_L)^T \in \mathbb{C}^{LMN}$, $\vec{\mathbf{w}} = (\mathbf{u}_0 + \mathbf{v}_1, \mathbf{v}_2, \dots, \mathbf{v}_L)^T \in \mathbb{C}^{LMN}$ and where the matrix $\mathbf{E} \in \mathbb{R}^{L \times L}$ has -1 on the lower sub-diagonal and zeros elsewhere, accounting for the transfer of the solution from one step to another.

2.2. The Paralpha algorithm. The system (2.5) is well posed as long as (2.4) is well posed and in order to solve it in an efficient way, one can use preconditioned Richardson iterations where the preconditioner is a diagonalizable block circulant Toeplitz matrix defined as

$$(2.6) \quad \mathbf{C}_\alpha := \mathbf{I}_L \otimes \mathbf{C}_{\text{coll}} + \mathbf{E}_\alpha \otimes \mathbf{H}, \quad \mathbf{E}_\alpha := \begin{bmatrix} 0 & & & -\alpha \\ -1 & 0 & & \\ & \ddots & \ddots & \\ & & -1 & 0 \end{bmatrix},$$

for $\alpha > 0$. This yields an iteration of the form

$$(2.7) \quad \mathbf{C}_\alpha \vec{\mathbf{u}}^{(k+1)} = (\mathbf{C}_\alpha - \mathbf{C}) \vec{\mathbf{u}}^{(k)} + \vec{\mathbf{w}}.$$

The following lemma explains the motivation for \mathbf{E}_α , leading to a diagonalizable preconditioner.

LEMMA 2.1. *The matrix $\mathbf{E}_\alpha \in \mathbb{R}^{L \times L}$ defined in (2.6) can be diagonalized as $\mathbf{E}_\alpha = \mathbf{V} \mathbf{D} \mathbf{V}^{-1}$, where $\mathbf{V} = \frac{1}{L} \mathbf{J} \mathbf{F}$ and*

$$\begin{aligned} \mathbf{D}_\alpha &= \text{diag}(d_1, \dots, d_L), d_l = -\alpha^{\frac{1}{L}} e^{-2\pi i \frac{l-1}{L}}, \\ \mathbf{J} &= \text{diag}(1, \alpha^{-\frac{1}{L}}, \dots, \alpha^{-\frac{L-1}{L}}) \\ [\mathbf{F}]_{jk} &= e^{2\pi i \frac{(j-1)(k-1)}{L}}, 1 \leq j, k \leq L, \\ \mathbf{V}^{-1} &= \mathbf{F}^* \mathbf{J}^{-1}. \end{aligned}$$

Proof. The proof can be found in [4]. \square

This particular diagonalization property of the preconditioner involving the scaled Fourier matrix allows parallelization across the time-steps [3] and it has been analyzed in many different ways [25, 26, 22, 15, 39]. The steps for performing one iteration as in (2.7) are then

$$(2.8a) \quad \vec{\mathbf{x}} = (\mathbf{V}^{-1} \otimes \mathbf{I}_{NM})((\mathbf{C}_\alpha - \mathbf{C}) \vec{\mathbf{u}}^{(k)} + \vec{\mathbf{w}}),$$

$$(2.8b) \quad (\mathbf{D}_\alpha \otimes \mathbf{H} + \mathbf{I}_L \otimes \mathbf{C}_{\text{coll}}) \vec{\mathbf{y}} = \vec{\mathbf{x}},$$

$$(2.8c) \quad \vec{\mathbf{u}}^{(k+1)} = (\mathbf{V} \otimes \mathbf{I}_{NM}) \vec{\mathbf{y}}.$$

Step (2.8b) can be performed in parallel since the matrix is block-diagonal while steps (2.8a) and (2.8c) can be computed with a parallel Fast Fourier transform (FFT) in time.

There still remains a question of how to solve the linear systems on the diagonal in (2.8b). For each step, they take the form

$$(d_l \mathbf{H} + \mathbf{C}_{\text{coll}}) \mathbf{y}_l = \mathbf{x}_l, \quad l = 1, \dots, L,$$

or in other words

$$(2.9) \quad ((d_l \mathbf{H}_M + \mathbf{I}_M) \otimes \mathbf{I}_N - \Delta T \mathbf{Q} \otimes \mathbf{A}) \mathbf{y}_l = \mathbf{x}_l, \quad i = 1, \dots, L.$$

Here $\mathbf{x}_l \in \mathbb{C}^{MN}$ denotes the l th block of the vector $\vec{\mathbf{x}} \in \mathbb{C}^{LMN}$. One way to approach this problem is to define $\mathbf{G}_l := d_l \mathbf{H}_M + \mathbf{I}_M$ for each $l = 1, \dots, L$. Then, \mathbf{G}_l is an

upper triangular matrix of size $M \times M$ and is nonsingular for $\alpha \neq 1$. Because of this, the linear systems in (2.9) can be rewritten in two steps as

$$(2.10a) \quad (\mathbf{I}_{MN} - \Delta T(\mathbf{Q}\mathbf{G}_l^{-1}) \otimes \mathbf{A})\mathbf{z}_l = \mathbf{x}_l,$$

$$(2.10b) \quad (\mathbf{G}_l \otimes \mathbf{I}_N)\mathbf{y}_l = \mathbf{z}_l.$$

Now, let's suppose that $\mathbf{Q}\mathbf{G}_l^{-1}$ is a diagonalizable matrix for a given l and α . Even though this statement is an assumption for now, the exact circumstances under which this is possible are discussed in section 3.3. If so, one can solve (2.10a) with diagonalizing a much smaller $M \times M$ matrix and inverting the matrices on the diagonal in parallel, but now across the quadrature nodes (or, as cast in [3], “across the method”). More precisely, let $\mathbf{Q}\mathbf{G}_l^{-1} = \mathbf{S}_l \mathbf{D}_l \mathbf{S}_l^{-1}$ denote the diagonal factorization, where $\mathbf{D}_l = \text{diag}(d_{l1}, \dots, d_{lM})$. Hence, the inner systems in (2.10a) can now be solved again in three steps for each $l = 1, \dots, L$ as

$$(2.11a) \quad (\mathbf{S}_l \otimes \mathbf{I}_N)\mathbf{x}_l^1 = \mathbf{x}_l,$$

$$(2.11b) \quad (\mathbf{I}_N - d_{lm}\Delta T\mathbf{A})\mathbf{x}_{lm}^2 = \mathbf{x}_{lm}^1, \quad m = 1, \dots, M,$$

$$(2.11c) \quad (\mathbf{S}_l^{-1} \otimes \mathbf{I}_N)\mathbf{z}_l = \mathbf{x}_l^2,$$

where $\mathbf{x}_{lm} \in \mathbb{C}^N$ denotes the m th block of $\mathbf{x}_l \in \mathbb{C}^{NM}$.

A summary of the full method is presented as a pseudo code in algorithm 2.1. It traces precisely the steps described above and indicates, which steps can be run in parallel. In this version, a different preconditioner is used in each iteration, defined by a given $(\alpha_k)_{k \in \mathbb{N}}$ sequence. A criterion when to stop as well as which sequence $(\alpha_k)_{k \in \mathbb{N}}$ to choose is discussed in the next section.

3. Parameter selection. After each iteration, a numerical error is introduced. This can be expressed and bounded as

$$(3.1) \quad \|\vec{\mathbf{u}}^{(k+1)} + \Delta \vec{\mathbf{u}}^{(k+1)} - \vec{\mathbf{u}}^*\| \leq c_\alpha \|\vec{\mathbf{u}}^{(k)} - \vec{\mathbf{u}}^*\| + \|\Delta \vec{\mathbf{u}}^{(k+1)}\|,$$

for some constant $c_\alpha > 0$. Moreover, we expect $\|\Delta \vec{\mathbf{u}}^{(k+1)}\| \rightarrow \infty$ and $c_\alpha \rightarrow 0$ when $\alpha \rightarrow 0$, making the decision on which parameter to choose for the next iteration more complicated. Bounding the second α -dependent term on the right side of (3.1) and approximating c_α would bring us closer in finding suitable α_{k+1} to use for the computation of $\vec{\mathbf{u}}^{(k+1)}$.

In order to formulate this problem in a more concrete way, we need to know how the error of the method behaves. This matter was dealt with in [39] and we shall present the convergence theorem for our case out of completeness.

THEOREM 3.1. *Assume that the matrix $\mathbf{A} \in \mathbb{C}^{N \times N}$ is diagonalizable as $\mathbf{A} = \mathbf{V}_A \mathbf{D}_A \mathbf{V}_A^{-1}$ and define $\mathbf{W} = \mathbf{I}_L \otimes \mathbf{V}_A$. Let \mathbf{u}^* denote the solution of the composite collocation problem (2.5). Then for any $k \geq 1$ it holds*

$$\|\vec{\mathbf{u}}^{(k+1)} - \vec{\mathbf{u}}^*\|_{\mathbf{W}, \infty} \leq \frac{\alpha}{1 - \alpha} \|\vec{\mathbf{u}}^{(k)} - \vec{\mathbf{u}}^*\|_{\mathbf{W}, \infty},$$

provided that the time-integrator (2.4) is stable and $\|\vec{\mathbf{u}}\|_{\mathbf{W}, \infty} = \|\mathbf{W}\vec{\mathbf{u}}\|_\infty$.

Proof. See [39, th. 2.2, def. 2.1]. \square

Algorithm 2.1 Paralpha with a given sequence of $(\alpha_k)_{k \in \mathbb{N}}$.

Input: $(\mathbf{C}_{\alpha_k})_{k \in \mathbb{N}}$, \mathbf{C} , $\vec{\mathbf{w}}$, $\vec{\mathbf{u}}^{(0)}$, tol
Output: a solution to $\mathbf{C}\vec{\mathbf{u}} = \vec{\mathbf{w}}$.

- 1: $k = 0$
- 2: **while** not done **do**
- 3: $\mathbf{D}_{\alpha_k} = \text{diag}(d_1, \dots, d_L)$, $d_l = -\alpha_k^{\frac{1}{L}} e^{-2\pi i \frac{l-1}{L}}$
- 4: $\vec{\mathbf{r}} = (\mathbf{C}_{\alpha_k} - \mathbf{C})\vec{\mathbf{u}}^{(k)} + \vec{\mathbf{w}}$
- 5: $\tilde{\vec{\mathbf{r}}} = (\mathbf{J}^{-1} \otimes \mathbf{I}_{NM})\vec{\mathbf{r}}$
- 6: $\vec{\mathbf{x}} = \text{FFT}(\tilde{\vec{\mathbf{r}}}_1, \dots, \tilde{\vec{\mathbf{r}}}_L)$
- 7: **for** $l = 1, \dots, L$ **in parallel do**
- 8: $\mathbf{G}_l = d_l \mathbf{H}_M + \mathbf{I}_M$
- 9: $\mathbf{Q}\mathbf{G}_l^{-1} = \mathbf{S}_l \mathbf{D}_l \mathbf{S}_l^{-1}$, $\mathbf{D}_l = \text{diag}(d_{l1}, \dots, d_{lm})$
- 10: $\mathbf{x}_l^1 = (\mathbf{S}_l^{-1} \otimes \mathbf{I}_N)\mathbf{x}_l$
- 11: **for** $m = 1, \dots, M$ **in parallel do**
- 12: **solve** $(\mathbf{I}_N - d_{lm} \Delta T \mathbf{A})\mathbf{x}_{lm}^2 = \mathbf{x}_{lm}^1$
- 13: **end for**
- 14: $\mathbf{z}_l = (\mathbf{S}_l \otimes \mathbf{I}_N)\mathbf{x}_l^2$
- 15: $\mathbf{y}_l = (\mathbf{G}_l^{-1} \otimes \mathbf{I}_N)\mathbf{z}_l$
- 16: **end for**
- 17: $\tilde{\vec{\mathbf{u}}}^{(k+1)} = \text{IFFT}(\mathbf{y}_1, \dots, \mathbf{y}_L)$
- 18: $\vec{\mathbf{u}}^{(k+1)} = (\mathbf{J} \otimes \mathbf{I}_{NM})\tilde{\vec{\mathbf{u}}}^{(k+1)}$
- 19: $k = k + 1$
- 20: **end while**
- 21: **return** $\vec{\mathbf{u}}^{(k)}$

Using the above result, we can write

$$\begin{aligned} \|\vec{\mathbf{u}}^{(k+1)} - \vec{\mathbf{u}}^*\|_\infty &\leq \|\mathbf{W}^{-1}\|_\infty \|\mathbf{W}(\vec{\mathbf{u}}^{(k+1)} - \vec{\mathbf{u}}^*)\|_\infty \\ &\leq \|\mathbf{W}^{-1}\| \frac{\alpha}{1-\alpha} \|\mathbf{W}(\vec{\mathbf{u}}^{(k)} - \vec{\mathbf{u}}^*)\|_\infty \\ &\leq \kappa_\infty(\mathbf{W}) \frac{\alpha}{1-\alpha} \|\vec{\mathbf{u}}^{(k)} - \vec{\mathbf{u}}^*\|_\infty. \end{aligned}$$

This then leaves the question of how to bound the second error term $\|\Delta\vec{\mathbf{u}}^{(k+1)}\|$ in equation (3.1).

3.1. Bounds for computation errors. The three steps in the diagonalization computation (2.8) can be generally analyzed in this order: a matrix-vector multiplication $y = \hat{\mathbf{A}}x$, solving a system $\hat{\mathbf{B}}z = y$ and again a matrix-vector multiplication $w = \hat{\mathbf{C}}z$, where in our particular case $\hat{\mathbf{C}}$ is the inverse of $\hat{\mathbf{A}}$. The following error bounds hold for any type of $\hat{\mathbf{A}}, \hat{\mathbf{B}}, \hat{\mathbf{C}} \in \mathbb{C}^{p \times p}$ and $x, y, z, w \in \mathbb{C}^p$, $p \in \mathbb{N}$, which is the reason behind this simplified notation. We assume that $\hat{\mathbf{B}}z = y$ represents the system solving of a block diagonal matrix, therefore we can say it represents each of the L system solves. The errors in play can be expressed as

$$(3.2a) \quad y + \Delta y = (\hat{\mathbf{A}} + \Delta \hat{\mathbf{A}})x$$

$$(3.2b) \quad (\hat{\mathbf{B}} + \Delta \hat{\mathbf{B}})(z + \Delta z) \approx y + \Delta y$$

$$(3.2c) \quad w + \Delta w = (\hat{\mathbf{C}} + \Delta \hat{\mathbf{C}})(z + \Delta z)$$

with relative errors satisfying

$$(3.3) \quad \|\Delta\hat{\mathbf{A}}\| \leq \varepsilon\|\hat{\mathbf{A}}\|, \|\Delta\hat{\mathbf{B}}\| \leq \varepsilon\|\hat{\mathbf{B}}\|, \|\Delta\hat{\mathbf{C}}\| \leq \varepsilon\|\hat{\mathbf{C}}\|,$$

for some $\varepsilon > 0$, representing machine precision.

LEMMA 3.2. *Let the system solve in (3.2b) be inexact, in other words $\|(\hat{\mathbf{B}} + \Delta\hat{\mathbf{B}})(z + \Delta z) - (y + \Delta y)\| \leq \tau\|y + \Delta y\|$ for some $\tau > 0$ and let (3.3) hold. Then the norm of the absolute error of w after the diagonalization process (3.2) satisfies*

$$\|\Delta w\| \leq \frac{\|\hat{\mathbf{B}}^{-1}\| \|\hat{\mathbf{A}}\| \|\hat{\mathbf{C}}\|}{1 - \varepsilon\kappa(\hat{\mathbf{B}})} (2\varepsilon + \tau + \varepsilon\kappa(\hat{\mathbf{B}}))\|x\| + O(\tau\varepsilon + \varepsilon^2),$$

where the matrix norm is consistent, i.e. $\|\hat{\mathbf{A}}x\| \leq \|\hat{\mathbf{A}}\|\|x\|$, and the condition number is norm induced with $\kappa(\hat{\mathbf{A}}) := \|\hat{\mathbf{A}}\|\|\hat{\mathbf{A}}^{-1}\|$.

Proof. See appendix A. \square

THEOREM 3.3. *After each iteration of Paralpfa for $\alpha \in (0, 1]$, under the assumption that the inner system solves in step (2.8b) satisfy $\|\hat{\mathbf{B}}(z + \Delta z) - (y + \Delta y)\|_\infty \leq \tau\|y + \Delta y\|$, the error of the $(k+1)$ th iterate can be bounded by*

$$(3.4) \quad \|\Delta\vec{\mathbf{u}}^{(k+1)}\|_\infty \leq \frac{\|\hat{\mathbf{B}}^{-1}\|_\infty}{1 - \varepsilon\kappa_\infty(\hat{\mathbf{B}})} \frac{L(2\varepsilon + \tau + \varepsilon\kappa_\infty(\hat{\mathbf{B}}))}{\alpha} \|\vec{\mathbf{r}}^{(k)}\|_\infty + O(\varepsilon\tau + \varepsilon^2),$$

where ε is machine precision as in (3.3), $\mathbf{r}^{(k)} = (\mathbf{C}_\alpha - \mathbf{C})\vec{\mathbf{u}}^{(k)} + \vec{\mathbf{w}}$ and $\hat{\mathbf{B}} = \mathbf{D} \otimes \mathbf{H} + \mathbf{I}_L \otimes \mathbf{C}_{\text{coll}}$. Furthermore, for $l = 1, \dots, L$ we have

$$(3.5) \quad \|\Delta\mathbf{u}_l^{(k+1)}\|_\infty \leq \frac{\|\hat{\mathbf{B}}^{-1}\|_\infty}{1 - \varepsilon\kappa_\infty(\hat{\mathbf{B}})} \alpha^{\frac{-(l-1)}{L}} L(2\varepsilon + \tau + \varepsilon\kappa_\infty(\hat{\mathbf{B}})) \|\vec{\mathbf{r}}^{(k)}\|_\infty + O(\varepsilon\tau + \varepsilon^2).$$

Proof. Let relation (3.3) hold. Define $\hat{\mathbf{A}} := \mathbf{V}^{-1} \otimes \mathbf{I}_{NM}$, $\hat{\mathbf{B}} = \mathbf{D} \otimes \mathbf{H} + \mathbf{I}_L \otimes \mathbf{C}_{\text{coll}}$ and $\hat{\mathbf{C}} := \mathbf{V} \otimes \mathbf{I}_{NM}$ where without loss of generality we can assume $\hat{\mathbf{A}} = \mathbf{V}^{-1}$ and $\hat{\mathbf{C}} = \mathbf{V}$. From lemma 2.1 we see that

$$\|\hat{\mathbf{A}}\|_\infty \|\hat{\mathbf{C}}\|_\infty \leq \frac{1}{L} \|\mathbf{J}\|_\infty \|\mathbf{J}^{-1}\|_\infty \|\mathbf{F}\|_\infty \|\mathbf{F}^*\|_\infty \leq \frac{L}{\alpha}$$

since $\|\mathbf{F}\|_\infty < L$ and $\|\mathbf{F}^*\|_\infty < L$. The proof for (3.4) now follows directly from lemma 3.2. Furthermore, if we define $\hat{\mathbf{A}} = \mathbf{V}^{-1}$ and $\hat{\mathbf{C}} = \frac{1}{L}\mathbf{F}$, then

$$\|\hat{\mathbf{A}}\|_\infty \|\hat{\mathbf{C}}\|_\infty \leq \frac{1}{L} \|\mathbf{J}^{-1}\|_\infty \|\mathbf{F}\|_\infty \|\mathbf{F}^*\| \leq L.$$

If now we define $\Delta w = (\mathbf{J}^{-1} \otimes \mathbf{I}_{MN})\Delta\vec{\mathbf{u}}^{(k+1)}$, we have

$$\|\mathbf{u}_l^{(k+1)}\|_\infty = \alpha^{\frac{-(l-1)}{L}} \|\Delta w_l\|_\infty \leq \alpha^{\frac{-(l-1)}{L}} \|\Delta w\|_\infty$$

and the proof for (3.5) again directly follows directly from lemma 3.2. \square

Remark 3.4. The IEEE standard guarantees that relation (3.3) holds for the infinity norm and some $\varepsilon = 2^{-p}$ representing machine precision.

The above theorem provides an idea how the round-off error propagates across the vector $\vec{\mathbf{u}}^{(k+1)}$. The larger the number of the time-steps, the larger the round-off error we can expect. This means that if the error between consecutive iterates is monitored, it is sufficient enough to do so just on the last time-step. Thus, we can avoid computing a residual and use the difference between two consecutive iterates at the last time-step as termination criterion.

3.2. Choosing the $(\alpha_k)_{k \in \mathbb{N}}$ sequence. While theorem 3.1 tells us that a small α will yield fast convergence, theorem 3.3 indicates that smaller α lead to larger numerical error per iteration. Suitable choices of α should balance both aspects.

In order to achieve that, define m_0 so that $\|\vec{\mathbf{u}}^{(0)} - \vec{\mathbf{u}}^*\|_\infty \approx m_0$. Using the results of theorems 3.1 and 3.3 we can approximate

$$\|\vec{\mathbf{u}}^{(1)} - \vec{\mathbf{u}}^*\|_\infty \lesssim \alpha m_0$$

and

$$\|\Delta \vec{\mathbf{u}}^{(1)}\|_\infty \lesssim \frac{\|\hat{\mathbf{B}}^{-1}\|_\infty}{1 - \varepsilon \kappa_\infty(\hat{\mathbf{B}})} \frac{L(2\varepsilon + \tau + \varepsilon \kappa_\infty(\hat{\mathbf{B}}))}{\alpha} \|\vec{\mathbf{r}}^{(0)}\|_\infty \lesssim \frac{L}{\alpha} (3\varepsilon + \tau) \|\vec{\mathbf{r}}^{(0)}\|_\infty,$$

where as before $\vec{\mathbf{r}}^{(0)} = (\mathbf{C}_\alpha - \mathbf{C})\vec{\mathbf{u}}^{(0)} + \vec{\mathbf{w}}$. Combining these estimates results, we have

$$(3.6) \quad \|\vec{\mathbf{u}}^{(1)} + \Delta \vec{\mathbf{u}}^{(1)} - \vec{\mathbf{u}}^*\|_\infty \lesssim \alpha m_0 + \frac{L}{\alpha} (3\varepsilon + \tau) \|\vec{\mathbf{r}}^{(0)}\|_\infty.$$

The aim is to find α such that the right-hand side of (3.6) is minimized for given L , ε and τ . Since $(\mathbf{C}_\alpha - \mathbf{C})\vec{\mathbf{u}}^{(0)}$ is a block vector with just $-\alpha \mathbf{H} \mathbf{u}_L^{(0)}$ being a nonzero block, we can treat the $\|\vec{\mathbf{r}}^{(0)}\|_\infty$ term in the minimization process roughly as $\|\vec{\mathbf{w}}\|_\infty$ since this part is more relevant. Defining $\gamma := L(3\varepsilon + \tau)\|\mathbf{w}\|_\infty$ for simplicity, we can state the problem as: finding the smallest $m_1 \in \mathbb{R}^+$ such that $m_1 = \alpha m_0 + \frac{\gamma}{\alpha}$, where $\alpha \in (0, 1]$. The solution is visible from the fact that $m_0 \alpha^2 - m_1 \alpha + \gamma = 0$ is a parabola with a discriminant $\Delta = m_1^2 - 4m_0\gamma$ and that the smallest value for m_1 so that $\Delta \geq 0$ is when $\Delta = 0$. This yields $m_1 = 2\sqrt{m_0\gamma}$ and a unique root $\alpha = \sqrt{\frac{\gamma}{m_0}}$. To interpret this result, we expect the error after one iteration to be around m_1 if the parameter $\alpha_1 = \sqrt{\frac{\gamma}{m_0}}$ is used. Recursively, we can approximate

$$\begin{aligned} \|\vec{\mathbf{u}}^{(k+1)} + \Delta \vec{\mathbf{u}}^{(k+1)} - \vec{\mathbf{u}}^*\| &\lesssim \|\vec{\mathbf{u}}^{(k+1)} - \vec{\mathbf{u}}^*\|_\infty + \frac{\gamma}{\alpha} \\ &\lesssim \alpha \|\vec{\mathbf{u}}^{(k)} + \Delta \vec{\mathbf{u}}^{(k)} - \vec{\mathbf{u}}^*\|_\infty + \frac{\gamma}{\alpha} \\ &\lesssim \alpha m_k + \frac{\gamma}{\alpha}. \end{aligned}$$

Solving the same minimization problem now for $m_{k+1} = \alpha m_k + \frac{\gamma}{\alpha}$ yields $m_{k+1} = 2\sqrt{m_k \gamma}$ and $\alpha = \alpha_{k+1} = \sqrt{\frac{\gamma}{m_k}}$.

If $4\gamma \leq m_k$ holds, then the approximations of errors m_k are descending. Now we can conclude that the sequence of $(\alpha_k)_{k \in \mathbb{N}}$ is ascending. Since $(\alpha_k)_{k \in \mathbb{N}}$ is additionally bounded from above with $\sqrt{\gamma/m_k} \leq 1/2$, we see that it is a convergent sequence with a limit in $(0, 1/2]$. Telescoping the recursion for m_k we get $m_k = (4\gamma)^{1-2^{-k}} m_0^{2^{-k}}$, $k \geq 1$, from where we see that the sequence is asymptotically bounded by 4γ . The convergence speed seems to be slower as the method iterates, but this does not have to be the case in practice. A remedy to this is to monitor the error of consecutive iterates and because of theorem 3.3 we can do so just for the last time-step. If this error is far lower than m_k , it is a good sign the convergence is much better than anticipated. Usually, monitoring just the error of consecutive iterates does not detect stagnation, but sees it as convergence. However, the combination of both can provide solid information. This discussion can be summarized in a following algorithm for the stopping criterion.

Algorithm 3.1 A stopping criterion combining approximations of worst case convergence and an error of consecutive iterates.

```

1:  $\gamma := L(3\varepsilon + \tau)\|\vec{\mathbf{w}}\|_\infty$ 
2:  $k = 0$ 
3: while  $m_k > \text{tol}$  do
4:    $m_{k+1} = 2\sqrt{m_k\gamma}$ 
5:    $\alpha_{k+1} = \sqrt{\gamma/m_k}$ 
6:    $\vec{\mathbf{u}}^{(k+1)} = \text{iterate}(\vec{\mathbf{u}}^{(k)}, m_{k+1}, \alpha_{k+1})$ 
7:   if  $\|\mathbf{u}_L^{(k+1)} - \mathbf{u}_L^{(k)}\|_\infty \leq \text{tol}$  then
8:     return  $\vec{\mathbf{u}}^{(k+1)}$ 
9:   end if
10:   $k = k + 1$ 
11: end while

```

The only problem remains how to approximate m_0 . Since it is an approximation of $\|\vec{\mathbf{u}}^{(0)} - \vec{\mathbf{u}}^*\|_\infty$ it is convenient to define a vector filled with initial conditions $\vec{\mathbf{u}}_0$ as the initial iterate $\vec{\mathbf{u}}^{(0)}$. Then, from the integral formulation, we have $m_0 \approx \max_{[0,T]} |u(t) - u(0)| \leq TL_u$ where L_u is the local Lipschitz constant of the solution on $[0, T]$. If this is inconvenient, one can also use that $m_0 \approx \|\vec{\mathbf{u}}^{(0)} - \vec{\mathbf{u}}^*\|_\infty \leq T \max_{[0,T]} \|Au(t) + b(t)\|_\infty \leq T(\|\mathbf{A}\|_\infty M_u + M_b)$ where M_u denotes the approximation of a maximum of the solution and M_b is the maximum for the function b . The best approximate convergence curves are when m_0 is a tight approximation. One can say that the errors are around values m_k as much as m_0 is around $\|\vec{\mathbf{u}}^{(0)} - \vec{\mathbf{u}}^*\|_\infty$. In practice, if m_0 was an upper bound, then all m_k were an upper bound.

This concludes the discussion about the $(\alpha_k)_{k \in \mathbb{N}}$ sequence. What we do not yet know is how to solve the inner systems after diagonalizing the preconditioner in (2.10a). The idea is to diagonalize $\mathbf{Q}\mathbf{G}_l^{-1}$ as well and pinpoint any problematic α for which this diagonalization is not possible.

3.3. Diagonalization of $\mathbf{Q}\mathbf{G}_l^{-1}$. In order to solve (2.10a) via diagonalization, we need to verify in which case it is possible to do such a factorization. It is known that a matrix is diagonalizable if its eigenvalues are distinct. Here we will show that for our matrix $\mathbf{Q}\mathbf{G}_l^{-1}$ it is also a necessary condition. Recall that $\mathbf{G}_l = d_l \mathbf{H}_M + \mathbf{I}_M$ is an upper triangular matrix with a computable inverse that is $\mathbf{G}_l^{-1} = \mathbf{I}_M - r_l \mathbf{H}_M$, where $r_l = d_l/(1 + d_l)$. We also know that $\mathbf{Q}\mathbf{H}_M = \mathbf{D}_t \mathbf{H}_M$, where $\mathbf{D}_t = \text{diag}(t_1, \dots, t_M)$. This last equation holds because the matrix is an integration matrix and integrates polynomials of degree $M - 1$ exactly. As a conclusion, we can write

$$(3.7) \quad \mathbf{Q}\mathbf{G}_l^{-1} = \mathbf{Q} - r_l \mathbf{D}_t \mathbf{H}_M.$$

To formulate the problem, we need to find $\lambda \in \mathbb{C}$ and $\mathbf{y} \neq 0$ such that $\mathbf{Q}\mathbf{G}_l^{-1}\mathbf{y} = \lambda\mathbf{y}$. Since applying \mathbf{Q} to a vector behaves like integrating a polynomial defined in the quadrature nodes (see (2.3)), we from now on look at a vector as an interpolation polynomial of degree $M - 1$ containing points (t_m, \mathbf{y}_m) , $m = 1, \dots, M$. Because of (3.7), the eigenproblem can now be reformulated as finding a polynomial h of degree $M - 1$ such that

$$\int_0^{t_m} h(s)ds + r_l t_m h(t_M) = \lambda h(t_m), \quad m = 1, \dots, M.$$

Substituting h with a derivative g' , where the polynomial g is of order M , yields

$$(3.8) \quad g(t_m) - g(0) + r_l t_m g'(t_M) = \lambda g'(t_m), \quad m = 1, \dots, M.$$

From here we see that the eigenvector represented as a polynomial g is not uniquely defined, because if g is a solution of (3.8), then $a_M g(t) + a_0$ is also a solution. Therefore, without loss of generality we can assume that g has the form

$$g(t) = t^M + a_{M-1} t^{M-1} + \dots + a_1 t.$$

As a consequence we have $g(0) = 0$. With these assumptions, g is uniquely defined since we have M nonlinear equations (3.8) and M unknowns $(a_{M-1}, \dots, a_1, \lambda)$. This is equivalent to the statement that an eigenproblem with distinct eigenvalues has a unique eigenvector if it is a unitary vector. This reformulation of the problem leads us to the following lemma.

LEMMA 3.5. *Define*

$$w_M(t) = (t - t_M) \dots (t - t_1) = t^M + b_{M-1} t^{M-1} + \dots + b_0.$$

Then, the eigenvalues of $\mathbf{Q}\mathbf{G}_l^{-1}$ are the roots of

$$p_M(\lambda) = M! \lambda^M + c_{M-1} \lambda^{M-1} + \dots + c_0,$$

where the coefficients are defined as $c_0 = (r_l + 1)b_0$,

$$c_m = m! b_m - r_l \sum_{j=1}^{M-m} \frac{(m+j)!}{j!} b_{m+j}, \quad 1 \leq m \leq M-1$$

and $b_M = 1$.

Proof. Without loss of generality one can assume $t_M = 1$. Summarizing the above discussion, the eigenproblem is equivalent to solving M nonlinear equations

$$(3.9) \quad g(t_m) + r_l t_m g'(1) - \lambda g'(t_m) = 0, \quad m = 1, \dots, M,$$

where $g(t) = t^M + a_{M-1} t^{M-1} + \dots + a_1 t$ and $\lambda \in \mathbb{C}$. Now we define

$$G(t) = g(t) + r_l t g'(1) - \lambda g'(t).$$

It holds that $G(t_m) = w_M(t_m)$ for $m = 1, \dots, M$ and that the difference $G - w_M$ is a polynomial of degree at most $M-1$, since both G and w_M are monic polynomials of degree M . Because $G - w_M$ is zero in M different points, we conclude that $G = w_M$. Equations (3.9) can compactly be rewritten as

$$(3.10) \quad g(t) + r_l t g'(1) - \lambda g'(t) = w_M(t).$$

Since the polynomial coefficients on the left-hand side of (3.10) are the same as on the right-hand side, we get

$$(*0) \quad -\lambda a_1 = b_0$$

$$(*1) \quad a_1 + r_l g'(1) - 2\lambda a_2 = b_1$$

$$(*2) \quad a_2 - 3\lambda a_3 = b_2$$

⋮

$$(*M-2) \quad a_{M-2} - (M-1)\lambda a_{M-1} = b_{M-2}$$

$$(*M-1) \quad a_{M-1} - M\lambda = b_{M-1}.$$

Telescoping these equations starting from (*M-1) up to (*m) for $m \geq 2$, we get

$$a_m = \sum_{j=0}^{M-m} \lambda^j \frac{(m+j)!}{m!} b_{m+j},$$

whereas from (*0) we get $a_1 = -b_0/\lambda$. Note that $\lambda \neq 0$ since both \mathbf{Q} and \mathbf{G}_l are nonsingular. The fact that \mathbf{Q} is a nonsingular matrix is visible because it is a mapping in a fashion

$$(3.12) \quad (t_1^m, \dots, t_M^m) \rightarrow \frac{1}{m+1} (t_1^{m+1}, \dots, t_M^{m+1}), \quad 0 \leq m \leq M-1.$$

The vectors in (3.12) form columns of the Vandermonde matrix \mathbf{W} which is known to be nonsingular when $0 < t_1 < \dots < t_M$. Because of (3.12), we have $\mathbf{QW} = \mathbf{D}_M \mathbf{W}$, where $\mathbf{D}_M = \text{diag}(1, 1/2, \dots, 1/M)$. Now, from here we see that \mathbf{Q} is nonsingular as a product of nonsingular matrices.

Substituting the expression for a_2 and a_1 into (*1) and multiplying it with $-\lambda \neq 0$ yields

$$(3.13) \quad -\lambda r_l g'(1) + \sum_{m=0}^M m! \lambda^m b_m = 0.$$

It remains to compute $g'(1)$. We have

$$\begin{aligned} g'(1) &= M + (M-1)a_{M-1} + \dots + 2a_2 + a_1 \\ &= M + \sum_{m=2}^{M-1} m \sum_{j=0}^{M-m} \lambda^j \frac{(m+j)!}{m!} b_{m+j} - \frac{b_0}{\lambda}, \end{aligned}$$

whereas

$$\lambda g'(1) = \sum_{m=2}^M \sum_{j=0}^{M-m} \lambda^{j+1} \frac{(m+j)!}{(m-1)!} b_{m+j} - b_0.$$

Now we have to shift the summations by 1 and reorder the summation

$$(3.14) \quad \lambda g'(1) + b_0 = \sum_{m=1}^{M-1} \sum_{j=1}^{M-m} \lambda^j \frac{(m+j)!}{m!} b_{m+j} = \sum_{j=1}^{M-1} \lambda^j \sum_{m=1}^{M-j} \frac{(m+j)!}{m!} b_{m+j}.$$

Combining (3.13) and (3.14) gives a polynomial in the λ variable with coefficients being exactly as stated in the lemma. \square

Remark 3.6. Because of equation (3.7), lemma 3.5 also gives a scaled characteristic polynomial p_M of an arbitrary Runge-Kutta matrix \mathbf{Q} in the special case when $r_l = 0$.

From the proof of lemma 3.5 it is visible that each λ generates exactly one polynomial g representing an eigenvector, therefore the matrix \mathbf{QG}_l^{-1} is diagonalizable if and only if the eigenvalues are distinct.

Lemma 3.5 also provides an analytic way of pinpointing the values r_l where \mathbf{QG}_l^{-1} is not diagonalizable. This can be done via obtaining the polynomial of roots for the Gauss-Radau quadrature as $R_M = P_{M-1} + P_M$, where P_M is the M th Legendre

polynomial which can be obtained with a recursive formula, see [38] for details. Since R_M has roots in the interval $[-1, 1]$ with the left point included, a linear substitution is required of form $x(t) = -2t+1$ to obtain the corresponding collocation nodes for the Gauss-Radau quadrature on $[0, 1]$. Then the monic polynomial colinear to $(R_M \circ x)(t)$ is exactly $w_M(t)$.

Now it remains to find the values of r_l for which p_M defined in lemma 3.5 has distinct roots. This can be done using the discriminant of the polynomial and computing these finitely many values since the discriminant of a polynomial Δ_{p_M} is nonzero if and only if the roots are distinct. The discriminant of a polynomial is defined as $\Delta_{p_M} = (-1)^{M(M-1)/2}/c_M \text{Res}(p_M, p'_M)$, and Res is the residual between two polynomials. Another option is to simply try it out during run time for a given α and numerically computing the roots of p_M . For $M = 2, 3$, we give the analysis here. Note that for $M = 1$, the diagonalization is already here since the matrix \mathbf{Q} is of size 1×1 .

EXAMPLE 1. When $M = 2$, the corresponding polynomial of roots is $w_2(t) = t^2 - \frac{4}{3}t + \frac{1}{3}$, generating $p_2(\lambda) = 2\lambda^2 - (\frac{4}{3} + 2r)\lambda + \frac{r+1}{3}$. Solving the equation $\Delta_{p_2} = 0$ is equivalent to $9r^2 + 6r - 2 = 0$ and the solutions are $r_* = \frac{-1 \pm 3\sqrt{3}}{13}$. Then, the matrix $\mathbf{Q}\mathbf{G}_l^{-1}$ is not diagonalizable for $\alpha_* \approx 0.323^L, 0.477^L$. These values are already of order $1e-8$ for $L \approx 25$ which is something unusable since it generates a too large round-off error for the outer diagonalization anyway.

EXAMPLE 2. When $M = 3$, the corresponding polynomial of roots is $w_3(t) = t^3 - \frac{9}{5}t^2 + \frac{9}{10}t - \frac{1}{10}$, generating $p_3(\lambda) = 6\lambda^3 - (\frac{18}{5} + 6r)\lambda^2 + (\frac{9}{10} + \frac{3}{5}r)\lambda - \frac{r+1}{10}$. Solving the equation $\Delta_{p_3} = 0$ is equivalent to $1700r^4 + 3560r^3 + 1872r^2 + 18r + 9 = 0$ and the solutions are $r_* \approx -1.0678, -1.0259, -0.000214 \pm 0.069518i$. This generates values $\alpha_* \approx 0.516^L, 0.504^L, 0.069^L$ which is already very small for $L \approx 25$.

In this chapter we have proposed an $(\alpha_k)_{k \in \mathbb{N}}$ sequence that is supposed to minimize the number of outer iterations, balancing the unwanted numerical errors and the convergence rate. We have identified those α_k around which the diagonalization of the inner method is not possible. Examples 1 and 2 show that for $M = 2, 3$ a sufficient number of time-steps L the diagonalization of $\mathbf{Q}\mathbf{G}_l^{-1}$ is possible for every time-step $[T_{l-1}, T_l], l = 1, \dots, L$. We also saw that the inner systems need to be solved very accurately. Theorem 3.3 indicates that the residual tolerance τ has to be of the order of the machine precision ε in order to be not the leading source of error. In the next section, we will discuss the actual implementation of Paralpha on a parallel machine.

4. Implementation. In this section an MPI-based parallel implementation is described in detail. This is the foundation of all the speedup and efficiency graphs presented in the results section, based on a code written in Python in the framework of `mpi4py` and `petsc4py` [6, 8, 7, 1].

4.1. Parallelization strategy. Lets suppose that the number of processors is $n_{\text{proc}} = n_{\text{step}}n_{\text{coll}}n_{\text{space}}$, where n_{step} processors handle the parallelization across the time-steps and $n_{\text{coll}}n_{\text{space}}$ processors handle parallelization of solving the collocation problem across the nodes as well as in space for each time step. The number of processors for time-step parallelism is $n_{\text{step}} = L$, where L is a power of 2. This means that each group of $n_{\text{coll}}n_{\text{space}}$ processor stores one approximation $\mathbf{u}_l^{(k)}$. Here $\mathbf{u}_l^{(k)} \in \mathbb{C}^{MN}$ denotes the corresponding time-step block of $\tilde{\mathbf{u}}^{(k)} \in \mathbb{C}^{LMN}$ defined in (2.7). For parallelization across the nodes, we let $n_{\text{coll}} = M$, so that exactly M groups of n_{space} processors deal with the collocation problem at each step. In

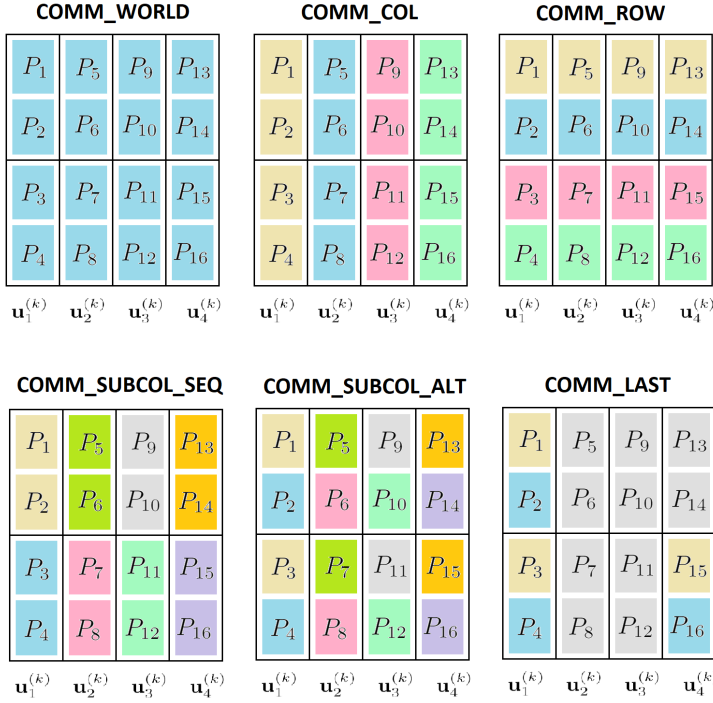


FIG. 1. This figure represents the communicating groups for $L = 4$ time-steps and the collocation method with $M = 2$ internal stages. There are $n_{\text{proc}} = 16$ processors of what $n_{\text{step}} = 4$, $n_{\text{coll}} = 2$ and $n_{\text{space}} = 2$. Each colored block is a part of the vector locally stored on a processor and the different color groups represents the subcommunicators of the MPI.COMM_WORLD. Each column of the table represents the storage for vector $\mathbf{u}_l^{(k)}$ whereas the upper and the lower parts of the column are for the two implicit stages of the collocation problem. In case when $n_{\text{coll}}n_{\text{space}} = M$, groups COMM_SUBCOL_SEQ and COMM_SUBCOL_ALT are nonexistent.

case $n_{\text{space}} = 1$, the each of the LM processors stores a single vector $u_m \in \mathbb{C}^N$ of $\mathbf{u}_l^{(k)} = (u_1, \dots, u_M)^T$, representing one implicit stage of the collocation problem. If $n_{\text{space}} > 1$, i.e. if spatial parallelism is used, then each of the LMn_{space} processors only stores a part of these implicit stages. See figure 1 for examples. We will describe the different communicators and communication steps in the following.

The diagonalization process can be seen as firstly computing (2.8a) (line 6 in algorithm 2.1) as a parallel FFT with a radix-2 algorithm on a scaled vector $(\tilde{\mathbf{r}}_1, \dots, \tilde{\mathbf{r}}_L)$. After that, each group of processors that stored $\tilde{\mathbf{r}}_l$ now holds \mathbf{x}_{l_i} , where the index l_i emerges from the butterfly structure which defines the communication scheme of radix-2 (see figure 2). At this stage the problem is decoupled, therefore there is no need to rearrange the vectors back in the original order as done in the standard radix-2 algorithm, which saves communication time. The inner system solves in (2.8b) can be carried out on these perturbed indices until the next radix-2 for the parallel IFFT in (2.8c) (line 17 in algorithm 2.1) is performed. The butterfly structure for communication is stretched across processors in the COMM_ROW subgroup and the communication cost is $O(2 \log_2(L))$ with chunks of memory sent and received being $O(MN/(n_{\text{coll}}n_{\text{space}}))$.

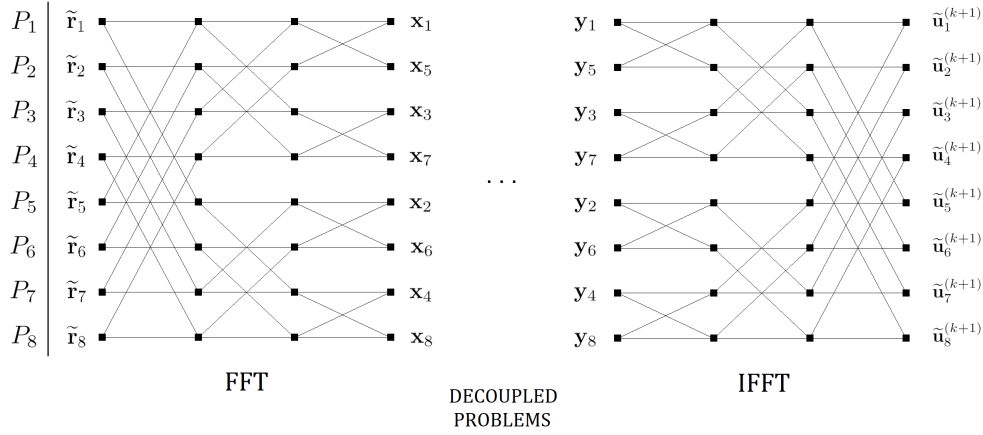


FIG. 2. An example of a radix-2 butterfly communication structure for $L = n_{\text{step}} = 8$ time-steps and processors. Because the indices after the forward Fourier transform do not need rearranging, the computation can carry on with the perturbed blocks of \mathbf{x}_{l_i} . The labeling here corresponds to the labeling of algorithm 2.1.

On the other hand, solving the diagonal systems in (2.8b) requires more care. Each group and subgroup of COMM_COL simultaneously and independently solves its own system, storing the solutions in \mathbf{y}_l . Excluding the communication time, this part is expected to be the most costly one. After forming and diagonalizing the matrix $\mathbf{Q}\mathbf{G}_l^{-1}$ locally on each processor, \mathbf{x}_l^1 as in (2.11a) (line 10 in algorithm 2.1) is firstly computed as

$$(\mathbf{x}_l^1)_m = \sum_{j=1}^M [\mathbf{S}_l^{-1}]_{mj} (\mathbf{x}_l)_j, \quad (\mathbf{x}_l^1)_m, (\mathbf{x}_l)_j \in \mathbb{C}^N, \quad \mathbf{S}_l \in \mathbb{C}^{M \times M},$$

where $(\mathbf{x}_l)_m$ is a subvector of $\mathbf{x}_l \in \mathbb{C}^{NM}$ containing indices from mN to $(m+1)N$ which represents the corresponding implicit collocation stage (parts of columns in figure 1 separated with black lines). In case $n_{\text{space}} > 1$, this summation can be computed via *reduce* on the COMM_SUBCOL_ALT level for each $m = 1, \dots, M$ making this action of complexity $O(M \log_2(M))$. If $n_{\text{coll}} \leq M$, then the communication complexity is $O(n_{\text{coll}} \log_2(n_{\text{coll}}))$ on the COMM_COL level with chunks of memory sent and received being $O(MN/(n_{\text{coll}} n_{\text{space}}))$ in both cases. Furthermore, equations (2.11c) and (2.10b) (lines 14 and 15 in algorithm 2.1) are computed in exactly the same manner as discussed above.

Finally, the inner linear systems after both diagonalizations in (2.11b) (line 12 in algorithm 2.1) are solved with the help of `petsc4py`. In case $n_{\text{coll}} \leq M$, each group of M/n_{coll} linear system is solved simultaneously, one by one on each processor, without additional processors passed on to `petsc4py`. If $n_{\text{space}} > 1$, then we have additional processors for handling the systems of size $N \times N$ in parallel on the COMM_SUBCOL_SEQ level which is passed on to `petsc4py` as a communicator. Here in this step, there is a lot of flexibility for defining the actual linear solver since `petsc4py` is a well developed library with a lot of different options. For our purpose, we make use of GMRES [32] without preconditioner.

4.2. Complexity and speedup analysis. In this section we will explore the theoretical speedup of parallelization in time with Paralpha. In order to do that, we need complexity estimates for three different cases:

$$\begin{aligned} T_{\text{seq}} &= L(MT_{\text{sol}} + 2M^2) = LM(T_{\text{sol}} + 2M), \\ T_{\text{Mpar}} &= L(T_{\text{sol}} + 2M \log(M)), \\ T_{\text{par}} &= k(T_{\text{sol,par}} + 2 \log(L) + 3M \log(M)). \end{aligned}$$

Here T_{seq} denotes the complexity when solving the collocation problem (2.4) sequentially over L time-steps directly via diagonalization of \mathbf{Q} . For each step, the solution is obtained by solving each system on the diagonal one by one M times with a solver complexity of T_{sol} . The expression $2M^2$ stands for the two matrix-vector multiplications needed for the diagonalization of \mathbf{Q} . T_{Mpar} denotes the complexity for solving the collocation problem sequentially over L time-steps via diagonalization, except these diagonal systems of complexity T_{sol} are solved in parallel across M processors. The two matrix-vector products can then be carried out in parallel with a complexity of $2M \log(M)$. At last, T_{par} represents the complexity of Paralpha with $n_{\text{step}} = L, n_{\text{coll}} = M$ processors. Here, k denotes the number of Paralpha iterations and $2 \log(L) + 3M \log(M)$ is the communication complexity as discussed in section 4.1. The solver complexity $T_{\text{sol,par}}$ may differ from T_{sol} since differently conditioned systems may be handled on the diagonals. Also, Paralpha requires to solve complex-valued problems even for real-valued systems, which could cause an overhead as well, depending on the solver at hand. Hence, the theoretical speedups for $k \in \mathbb{N}$ iterations look like this:

$$(4.1a) \quad \frac{T_{\text{seq}}}{T_{\text{par}}} = \frac{LM(T_{\text{sol}} + 2M)}{k(T_{\text{sol,par}} + 2 \log(L) + 3M \log(M))},$$

$$(4.1b) \quad \frac{T_{\text{Mpar}}}{T_{\text{par}}} = \frac{L(T_{\text{sol}} + 2M \log(M))}{k(T_{\text{sol,par}} + 2 \log(L) + 3M \log(M))}.$$

The true definition of speedup would be (4.1a), however the baseline method in Paralpha is also a parallel method and so we also need to take (4.1b) into account. For $L \geq 2$ we have

$$2 \log(L) + 3M \log(M) \geq 2M$$

which in combination with (4.1a) gives

$$(4.2) \quad \frac{T_{\text{seq}}}{T_{\text{par}}} \leq \frac{LM}{k} \frac{T_{\text{sol}} + 2M}{T_{\text{sol,par}} + 2M}.$$

If we combine the fact that

$$2 \log(L) + 3M \log(M) \geq 2M \log(M)$$

is true for all M, L and (4.1b), we get

$$(4.3) \quad \frac{T_{\text{Mpar}}}{T_{\text{par}}} \leq \frac{L}{k} \frac{T_{\text{sol}} + 2M \log(M)}{T_{\text{sol,par}} + 2M \log(M)}.$$

We can see that these speedup estimates (4.2) and (4.3) roughly depend on the ratio between how many steps and nodes are handled in parallel and the number of

Paralpha iterations. This is not a surprise when dealing with Parareal-based parallel-in-time methods and our speedup estimates fit the usual theoretical bounds in this field, too. Most importantly, as in Parareal, is crucial to minimize the number of iterations in order to achieve parallel performance. With the $(\alpha_k)_{k \in \mathbb{N}}$ sequence defined in Section 3.2, this goal can be achieved, as we will see in the following section.

5. Numerical results. We study the behavior of Paralpha for two different linear test problems. All results shown here were obtained with our Python implementation of Paralpha, which can be found on GitHub [37]. The first test equation is the heat equation, governed by

$$(5.1) \quad u_t = \Delta u + \sin(2\pi x) \sin(2\pi y) (8\pi^2 \cos(t) - \sin(t)), \text{ on } [\pi, \pi + T] \times [0, 1]^2,$$

and the exact solution is $u(t, x, y) = \sin(t) \sin(2\pi x) \sin(2\pi y)$. This equation has periodic boundary conditions which were used to form the discrete periodic Laplacian with central differences bringing the equation in the generic form (2.1).

The second PDE is the advection equation defined as

$$(5.2) \quad u_t + u_x + u_y = 0, \text{ on } [0, T] \times [0, 1]^2,$$

with a solution $u(t, x, y) = \sin(2\pi x - 2\pi t) \sin(2\pi y - 2\pi t)$. Here we again have periodicity on the boundaries which was used to form an upwind scheme.

All tests shown here were performed on the supercomputer JUWELS [21].

5.1. Counting iterations. The theoretical background of section 3.2 is verified for the advection equation. The numbers of discretization points in space and time are chosen so that the error with respect to the exact solution (infinity norm) is below 10^{-12} , without overresolving in space or time. The complete setup is $T = 0.0128$, $L = 64$, $M = 3$, 5th-order upwind scheme in space with $N = 700$. The inner solver is GMRES with a relative tolerance $\tau = 10^{-15}$. Figure 3 compares the convergence when the $(\alpha_k)_{k \in \mathbb{N}}$ sequence is used from algorithm 3.2 to the convergence when each fixed α_k from that sequence is used individually for the full run. For larger α values we can see a slow convergence curve that can reach better accuracy while for a smaller α values the convergence is extremely steep, but short living. Using the $(\alpha_k)_{k \in \mathbb{N}}$ sequence is clearly superior compared to a fixed α . The test for the heat equation looks very similar and is not shown here.

Understanding the convergence behavior allows us to roughly predict the number of iterations for a given threshold. In order to be able to compare the convergence of the method, we have to test it when solving the same initial value problem with the same domain for three thresholds 10^{-5} , 10^{-9} , 10^{-12} . One challenge for an actual application is the question when to stop the iteration of Paralpha, since the actual error is not available. As discussed in section 3.1, a valid candidate is the difference between two iterates at the last time-step, cf. lemma 3.2. To check the impact of this choice, figure 4 shows the convergence behavior for the two test problem with the adaptive- α strategy, both for the actual errors and for the difference between two iterates. The discretization parameters for each threshold are chosen accordingly for a fixed T (see table 1 for details).

5.2. Parallel scaling. After obtaining an intuition how Paralpha converges and verifying the effectiveness of our adaptive strategy for selecting α_k , we now measure the actual speedup of the method for our two equations and the three different thresholds 10^{-5} , 10^{-9} , 10^{-12} . The idea is to compare the execution time of 64 sequential

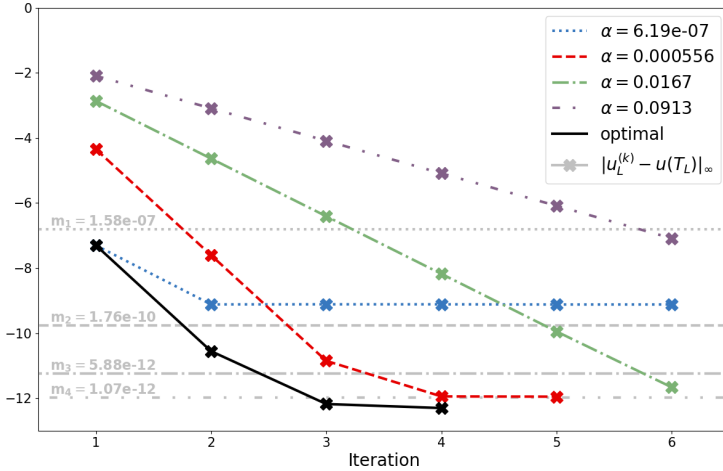


FIG. 3. Adaptive strategy vs. convergence for fixed α_k from the sequence. The y-axis represents the error in \log_{10} scale whereas the vertical lines represent the m_k sequence starting with $m_0 = 10\Delta T$. The solid line is the convergence history with the sequence of α_k given as $(6.19 \times 10^{-7}, 0.000556, 0.0167, 0.0913)$.

	Heat, $T = 0.1$			Advection, $T = 10^{-2}$		
	10^{-5}	10^{-9}	10^{-12}	10^{-5}	10^{-9}	10^{-12}
tol	10^{-5}	10^{-9}	10^{-12}	10^{-5}	10^{-9}	10^{-12}
N	450	400	300	350	350	490
κ	2	4	6	2	4	5
M	1	2	3	2	2	3
L	32	32	16	8	16	32
τ	10^{-6}	10^{-10}	10^{-13}	10^{-8}	10^{-11}	$5 \cdot 10^{-14}$

TABLE 1

Parameter choice depending on the equation in order to reach an error $\|\mathbf{u}(T) - \mathbf{u}_L\|_\infty < \text{tol}$ when solving with a standard sequential approach. κ denotes the discretization order in space, where upwind was chosen for the advection equation and centered differences for the heat equation.

steps solving the collocation problem via diagonalization of \mathbf{Q} to Paralpha, handling $L = 1, 2, \dots, 64$ time-steps at once. In other words, Paralpha is used as a parallel solver for a block of L steps and repeatedly applied in a sequential way until all the 64 time-steps are covered. For each run, $\Delta T = T_{64}/64$ was fixed while L varies (see table 2 for details). The number of spatial and temporal discretization points are chosen in a way so that the method does not overresolve in space nor time (see table 2 for details). Note that the timings do not include the startup time, the setup nor output times.

The linear system solver used for the test runs is GMRES with a relative stopping tolerance τ . An advantage of using an iterative solver in a sequential run is that τ can be just a bit smaller than the desired threshold we want to reach on our domain, otherwise it would unnecessarily prolong the runtime. However, this is not the case when choosing a relative tolerance $\tilde{\tau}$ for the linear solver within Paralpha (see algorithm 3.2, figure 3 and section 4.2). On the one hand, Paralpha benefits strongly from having a small $\tilde{\tau}$ in general since it plays a key role in the convergence, as we saw in lemma 3.2. On the other hand, the linear solver then needs more iterations and execution time $T_{\text{sol,par}}$ is higher, cf. 4.2. As a result, this is indeed a drawback when using Paralpha and has to be kept in mind.

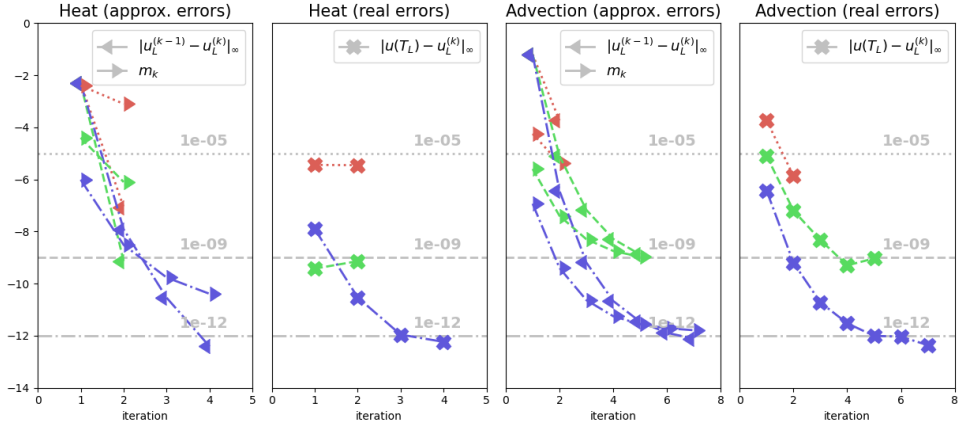


FIG. 4. *Convergence with the adaptive strategy for different thresholds.* The y-axis represents the error in \log_{10} scale and vertical lines represent the thresholds for the stopping criterion. 'approx. errors' graphs contain the information available on runtime which are: the errors of consecutive iterates in the last time-step and the approximations of the upper bound for the error in each iteration, the m_k values starting with $m_0 = \Delta T$.

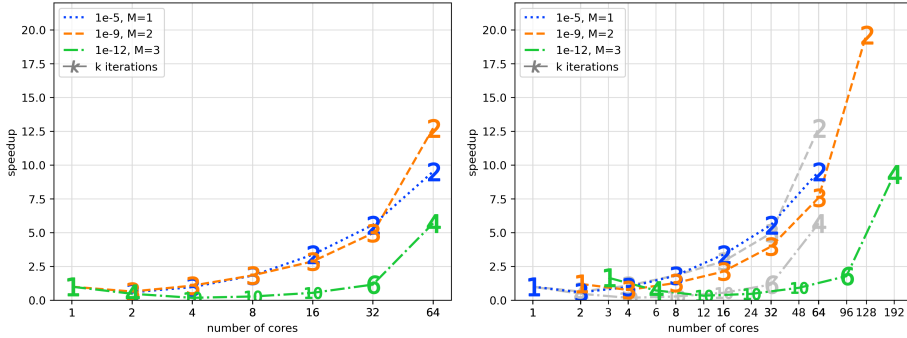
	Heat			Advection		
tol	10^{-5}	10^{-9}	10^{-12}	10^{-5}	10^{-9}	10^{-12}
N	350	400	350	800	800	700
κ	2	4	6	1	3	5
M	1	2	3	1	2	3
T_{64}	0.32	0.16	0.16	0.00016	0.00064	0.0128
τ	10^{-6}	10^{-10}	10^{-14}	10^{-6}	10^{-11}	10^{-14}
$\tilde{\tau}$	10^{-6}	10^{-10}	10^{-13}	10^{-9}	10^{-13}	10^{-15}

TABLE 2

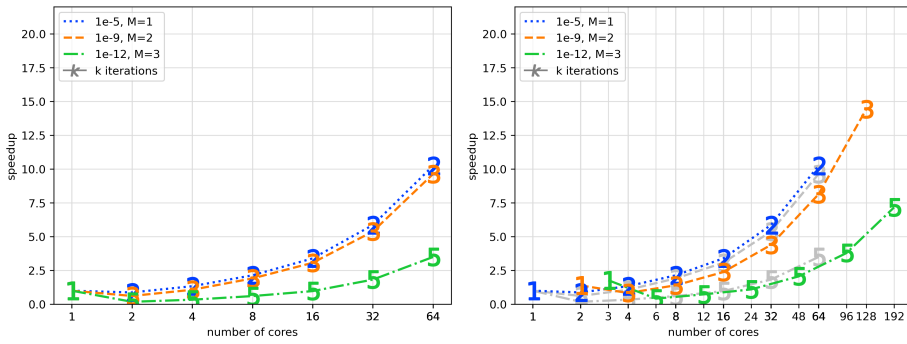
Parameter choice depending on the equation in order to reach an error $\|\mathbf{u}(T) - \mathbf{u}_L\|_\infty < \text{tol}$ when solving with a standard sequential approach. Here κ denotes the discretization order in space, where upwind was chosen for the advection equation and centered differences for the heat equation. Here T_{64} represents the interval length that is needed so that the error is below tol after 64 time-steps.

The strong scaling plots for Paralpha running parallel across time-steps and parallel across quadrature nodes are presented in figure 5. We can see that Paralpha provides significant speedup for both heat and advection equation. It also becomes clear that when very accurate results are needed (green curves), the performance is degrading. Interestingly, this is in contrast to methods like PFASST or RIDC [28], where higher order in time gives better parallel performance. Comparing parallelization strategies, using both parallelization across the quadrature nodes and time-steps leads to better results and is always preferable. The results do not differ much between heat and advection equation, showing only slightly worse results for the latter. This supports the idea that single-level diagonalization as done in Paralpha is a promising strategy also for hyperbolic problems. Note, however, that for the heat equation we have multiple runs with up to 10 iterations. This is because the linear system shifts that are produced by the diagonalization procedure are poorly conditioned for the particular choice of the α_k . Manually picking this sequence with slightly different, larger values can circumvent this issue. This is not done here and a more in-depth study of this phenomenon is left for future work.

Yet, parallel-in-time integration methods are ideally used in combination with a



(a) Heat equation



(b) Advection equation

FIG. 5. Strong scaling plots for the three thresholds and two equations. The numbers on the graphs show the number of iterations Paralpha needs in order to reach the given tolerance. The left graphs show a setup where $L = n_{\text{step}}$ and $n_{\text{coll}} = 1$ whereas the graphs in the right are when $L = n_{\text{step}}$ and $M = n_{\text{coll}}$ (first n_{coll} cores are used for the parallelization across the quadrature nodes). In both cases $n_{\text{space}} = 1$, i.e. there is no spatial parallelization. The gray plots on are the same as in the left column, serving as reference information.

space-parallel algorithm, especially in the field of PDE solvers. We therefore test Paralpha together with `petsc4py`'s parallel implementation of GMRES for the advection equation. The results are shown in figure 6. The number of cores for spatial scaling was chosen in a way so that we firstly scaled `petsc4py` when solving sequentially with implicit Euler on 64 time-steps and then chose the number of cores $n_{\text{space}} = 12$ as the last point where `petsc4py` scaled reasonably well for this problem size. With this setup fixed, the strong scaling across all quadrature nodes and time-steps is repeated for $L = 1, 2, \dots, 64$ for three different thresholds $10^{-5}, 10^{-9}, 10^{-12}$. The plots show clearly that using Paralpha we can get significant higher speedups for a fixed size problem than when using a space-parallel solver only. In the best case presented here, we obtain a speedup of about 85 over the sequential run. We would like to emphasize here that all runs are done with realistic parameters, not resolving in space, time or in the inner solves [16]. Thus, while the space-parallel solver gives speedup of up to about 8, we can get another factor of more than 10 by using a space- and doubly time-parallel method.

6. Conclusion. In this paper an implementation of a diagonalization-based parallel-in-time integrator is presented. Going from the theoretical description and

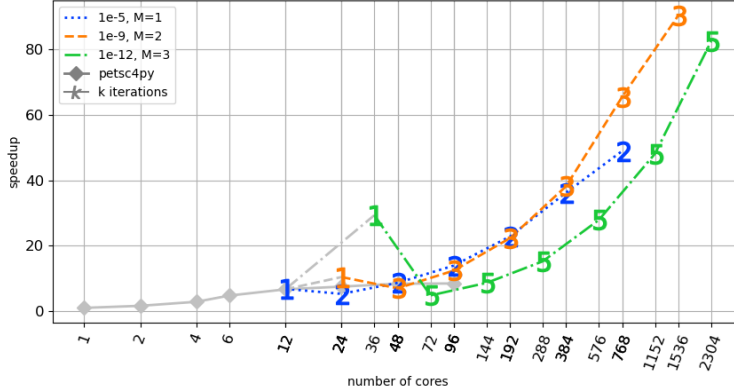


FIG. 6. Strong scaling plots for the advection equation and three thresholds. The solid gray line represents the spatial scaling with `petsc4py` for the advection equation solved sequentially with implicit Euler on 64 time-steps. The curve shows the scaling of `petsc4py` for our problem is best around 12 cores, since using more cores does not increase the speedup much. The colored lines represent the scaling where $n_{\text{step}} = L$, $n_{\text{coll}} = M$ and $n_{\text{space}} = 12$. The numbers on the graphs represent the number of iterations Paralpha needs in order to reach the given tolerance.

analysis of these methods to an actual parallel implementation yields quite a few expected and some unexpected challenges. Using an α -circulant, all-at-once preconditioner for a simple Richardson iteration, the diagonalization of this preconditioner leads to an appealing time-parallel method without the need to find a suitable coarsening strategy. We extend this idea to collocation problems and show a way to solve the local problems on each time-step efficiently again in parallel, making this method doubly-parallel-in-time. Based on convergence theory and error bounds, we propose an effective and applicable strategy to adaptively select the crucial α parameter for each iteration. However, depending on the size of the collocation problem, we show that some of these α lead to non-diagonalizable inner systems, which need to be avoided. This theoretical part is augmented by a thorough description of the parallel implementation, which is named Paralpha. We estimate the expected speedup, provide a verification of the adaptive choice of the parameters and, finally, show actual parallel runs on a high-performance computing system on up to 2304 cores. These parallel test demonstrate that Paralpha does indeed yield a significant decrease of time-to-solution, even far beyond the point of saturation of spatial parallelization.

By design, the diagonalization-based parallel-in-time integrators work only for linear problems with constant coefficients. In order to solve more complex, more realistic problems, they have to be coupled to e.g. Newton methods. Here, they work as inner solvers for an inexact outer Newton iteration. As such, the challenges and their solutions presented here are still valid. The obvious next step is to extend this implementation and the results to nonlinear problems, using the existing theory from the literature and our own extensions as described in this paper.

Appendix A. Proof of lemma 3.2.

With $\hat{\mathbf{C}}z = w$ it holds

$$\Delta w = \hat{\mathbf{C}}\Delta z + \Delta\hat{\mathbf{C}}(z + \Delta z),$$

from where

$$(A.1) \quad \|\Delta w\| \leq \|\hat{\mathbf{C}}\| \|\Delta z\| + \varepsilon \|\hat{\mathbf{C}}\| \|\Delta z + z\|.$$

Now we need to find a way to bound $\|\Delta z\|$ and $\|\Delta z + z\|$. Since the system solving is inexact, there exists a vector ξ such that $(\hat{\mathbf{B}} + \Delta\hat{\mathbf{B}})(z + \Delta z) = y + \Delta y + \xi$ and $\|\xi\| \leq \tau \|y + \Delta y\|$. From here we have $(\hat{\mathbf{B}} + \Delta\hat{\mathbf{B}})\Delta z + \Delta\hat{\mathbf{B}}z = \Delta y + \xi$ and thus

$$\Delta z = (\hat{\mathbf{B}} + \Delta\hat{\mathbf{B}})^{-1}(\Delta y + \xi - \Delta\hat{\mathbf{B}}z)$$

which yields the bound

$$(A.2) \quad \begin{aligned} \|\Delta z\| &\leq \|(\hat{\mathbf{B}} + \Delta\hat{\mathbf{B}})^{-1}\| (\|\Delta y\| + \|\xi\| + \varepsilon \|\hat{\mathbf{B}}\| \|z\|) \\ &\leq \|(\hat{\mathbf{B}} + \Delta\hat{\mathbf{B}})^{-1}\| (\|\Delta y\| + \tau \|\Delta y + y\| + \varepsilon \kappa(\hat{\mathbf{B}}) \|y\|), \end{aligned}$$

where the last inequality comes from the fact that $\|z\| \leq \|\hat{\mathbf{B}}^{-1}\| \|y\|$. Note that $\hat{\mathbf{B}} + \Delta\hat{\mathbf{B}}$ is invertible for small perturbations if $\hat{\mathbf{B}}$ is invertible. On the other hand, we have

$$z + \Delta z = (\hat{\mathbf{B}} + \Delta\hat{\mathbf{B}})^{-1}(y + \Delta y + \xi)$$

which gives

$$(A.3) \quad \begin{aligned} \|z + \Delta z\| &\leq \|(\hat{\mathbf{B}} + \Delta\hat{\mathbf{B}})^{-1}\| (\|y + \Delta y\| + \|\xi\|) \\ &\leq (1 + \tau) \|(\hat{\mathbf{B}} + \Delta\hat{\mathbf{B}})^{-1}\| \|y + \Delta y\|. \end{aligned}$$

Combining (A.2) and (A.3) with (A.1) yields

$$(A.4) \quad \|\Delta w\| \leq \|(\hat{\mathbf{B}} + \Delta\hat{\mathbf{B}})^{-1}\| \|\hat{\mathbf{C}}\| (\|\Delta y\| + (\tau + \varepsilon + \varepsilon\tau) \|y + \Delta y\| + \varepsilon \kappa(\hat{\mathbf{B}}) \|y\|).$$

Since $y = \hat{\mathbf{A}}x$ and $\|\Delta\hat{\mathbf{A}}\| \leq \varepsilon \|\hat{\mathbf{A}}\|$, we get the inequalities

$$\begin{aligned} \|y\| &\leq \|\hat{\mathbf{A}}\| \|x\|, \\ \|\Delta y\| &= \|\Delta\hat{\mathbf{A}}x\| \leq \varepsilon \|\hat{\mathbf{A}}\| \|x\|, \\ \|y + \Delta y\| &\leq (1 + \varepsilon) \|\hat{\mathbf{A}}\| \|x\|. \end{aligned}$$

Including these inequalities in (A.4) yields

$$\begin{aligned} \|\Delta w\| &\leq \|(\hat{\mathbf{B}} + \Delta\hat{\mathbf{B}})^{-1}\| \|\hat{\mathbf{C}}\| \|\hat{\mathbf{A}}\| (\varepsilon + (\tau + \varepsilon + \varepsilon\tau)(1 + \varepsilon) + \varepsilon \kappa(\hat{\mathbf{B}})) \|x\| \\ &\leq \|(\hat{\mathbf{B}} + \Delta\hat{\mathbf{B}})^{-1}\| \|\hat{\mathbf{C}}\| \|\hat{\mathbf{A}}\| (2\varepsilon + \tau + \varepsilon \kappa(\hat{\mathbf{B}})) \|x\| + O(\varepsilon\tau + \varepsilon^2). \end{aligned}$$

It just remains to bound $\|(\hat{\mathbf{B}} + \Delta\hat{\mathbf{B}})^{-1}\|$. From relation $(\hat{\mathbf{B}} + \Delta\hat{\mathbf{B}})^{-1} = \hat{\mathbf{B}}^{-1}(\mathbf{I} + \hat{\mathbf{B}}^{-1}\Delta\hat{\mathbf{B}})^{-1}$ we have

$$\|(\hat{\mathbf{B}} + \Delta\hat{\mathbf{B}})^{-1}\| \leq \|\hat{\mathbf{B}}^{-1}\| \|(\mathbf{I} + \hat{\mathbf{B}}^{-1}\Delta\hat{\mathbf{B}})^{-1}\| \leq \frac{\|\hat{\mathbf{B}}^{-1}\|}{1 - \|\hat{\mathbf{B}}^{-1}\Delta\hat{\mathbf{B}}\|}.$$

Since the function $1/(1 - x)$ is monotonically increasing, we get

$$\|(\hat{\mathbf{B}} + \Delta\hat{\mathbf{B}})^{-1}\| \leq \frac{\|\hat{\mathbf{B}}^{-1}\|}{1 - \varepsilon \kappa(\hat{\mathbf{B}})}$$

which completes the proof.

REFERENCES

- [1] S. BALAY, S. ABHYANKAR, M. ADAMS, J. BROWN, P. BRUNE, K. BUSCHELMAN, L. DALCIN, A. DENER, V. EJKHOUT, W. GROPP, D. KARPEYEV, D. KAUSHIK, M. KNEPLEY, D. MAY, L. C. MCINNES, R. MILLS, T. MUNSON, K. RUPP, P. SANAN, B. SMITH, S. ZAMPINI, H. ZHANG, AND H. ZHANG, *PETSc Users Manual*, 2020, <http://www.mcs.anl.gov/petsc/petsc-current/docs/manual.pdf>. ANL-95/11 - Revision 3.13.
- [2] H. BRUNNER, *Volterra Integral Equations An Introduction to Theory and Applications*, Cambridge Monographs on Applied and Computational Mathematics, Cambridge University Press, 2017, <https://doi.org/10.1017/9781316162491>.
- [3] K. BURRAGE, *Parallel methods for ODEs*, Advances in Computational Mathematics, 7 (1997), pp. 1–3.
- [4] R. E. CLINE, R. J. PLEMMONS, AND G. WORM, *Generalized inverses of certain Toeplitz matrices*, Linear Algebra and its Applications, 8(1) (1974), pp. 25–33, [https://doi.org/10.1016/0024-3795\(74\)90004-4](https://doi.org/10.1016/0024-3795(74)90004-4).
- [5] X. DAI AND Y. MADAY, *Stable Parareal in Time Method for Firstand Second-Order Hyperbolic Systems*, SIAM Journal on Scientific Computing, 5(1) (2013), p. A52–A78, <https://doi.org/10.1137/110861002>.
- [6] L. DALCIN, P. KLER, R. PAZ, AND A. COSIMO, *Parallel Distributed Computing using Python*, Advances in Water Resources, 34(9) (2011), pp. 1124–1139. <http://dx.doi.org/10.1016/j.advwatres.2011.04.013>.
- [7] L. DALCIN, R. PAZ, AND M. STORTI, *MPI for Python*, Journal of Parallel and Distributed Computing, 65(9) (2005), pp. 1108–1115. <http://dx.doi.org/10.1016/j.jpdc.2005.03.010>.
- [8] L. DALCIN, R. PAZ, M. STORTI, AND J. D’ELIA, *MPI for Python: performance improvements and MPI-2 extensions*, Journal of Parallel and Distributed Computing, 68(5) (2008), pp. 655–662. <http://dx.doi.org/10.1016/j.jpdc.2007.09.005>.
- [9] M. EMMETT AND M. L. MINION, *Toward an Efficient Parallel in Time Method for Partial Differential Equations*, Communications in Applied Mathematics and Computational Science, 7 (2012), pp. 105–132, <https://doi.org/10.2140/camcos.2012.7.105>, <http://dx.doi.org/10.2140/camcos.2012.7.105>.
- [10] R. FALGOUT, S. FRIEDHOFF, T. KOLEV, S. MACLACHLAN, AND J. SCHRODER, *Parallel Time Integration with Multigrid*, SIAM Journal on Scientific Computing, 36 (6) (2014), p. C635–C661, <https://doi.org/10.1137/130944230>.
- [11] M. J. GANDER, *50 Years of Time Parallel Time Integration*, in Multiple Shooting and Time Domain Decomposition Methods, T. Carraro, M. Geiger, S. Körkel, and R. Rannacher, eds., vol. 9 of Contributions in Mathematical and Computational Sciences, Springer, Cham, 2015, https://doi.org/10.1007/978-3-319-23321-5_3.
- [12] M. J. GANDER AND S. GÜTTEL, *PARAEXP: A Parallel Integrator for Linear Initial-Value Problems*, SIAM Journal on Scientific Computing, 35(2) (2013), p. C123–C142, <https://doi.org/10.1137/110856137>.
- [13] M. J. GANDER AND M. PETCU, *Analysis of a Krylov Subspace Enhanced Parareal Algorithm for Linear Problem*, ESAIM, 25 (2008), p. 114–129, <https://doi.org/10.1051/proc:082508>.
- [14] M. J. GANDER AND S. VANDEWALLE, *On the Superlinear and Linear Convergence of the Parareal Algorithm*, in Domain Decomposition Methods in Science and Engineering, Lecture Notes in Computational Science and Engineering, O. Widlund and D. Keyes, eds., vol. 55, Springer Berlin Heidelberg, 2007, p. 291–298, https://doi.org/10.1007/978-3-540-34469-8_34.
- [15] M. J. GANDER AND S.-L. WU, *A Diagonalization-Based Parareal Algorithm for Dissipative and Wave Propagation Problems*, SIAM J. Numer. Anal., 58(5) (2020), p. 2981–3009, <https://doi.org/10.1137/19M1271683>.
- [16] S. GOETSCHEL, M. MINION, D. RUPRECHT, AND R. SPECK, *Twelve Ways To Fool The Masses When Giving Parallel-In-Time Results*. unpublished, 2021, <https://arxiv.org/abs/2102.11670>.
- [17] J. HAHNE, S. FRIEDHOFF, AND M. BOLTEN, *Pymgrit: A python package for the parallel-in-time method mgrit*. unpublished, 2020, <http://arxiv.org/abs/2008.05172v1>.
- [18] E. HAIRER AND G. WANNER, *Solving Ordinary Differential Equations II*, Springer Series in Computational Mathematics, Springer, Berlin, Heidelberg, 1996, <https://doi.org/10.1007/978-3-642-05221-7>.
- [19] T. S. HAUT, T. BABB, P. G. MARTINSSON, AND B. A. WINGATE, *A high-order time-parallel scheme for solving wave propagation problems via the direct construction of an approximate time-evolution operator*, IMA Journal of Numerical Analysis, 36(2) (2016), p. 688–716, <https://doi.org/10.1093/imanum/drv021>.

[20] J. L. LIONS AND Y. MADAY AND G. TURINICI, *A "parareal" in time discretization of PDE's*, Comptes Rendus de l'Académie des Sciences, Série I, 332 (7) (2001), p. 661–668, [https://doi.org/10.1016/S0764-4442\(00\)01793-6](https://doi.org/10.1016/S0764-4442(00)01793-6).

[21] JÜLICH SUPERCOMPUTING CENTRE, *JUWELS: Modular Tier-0/1 Supercomputer at the Jülich Supercomputing Centre*, Journal of large-scale research facilities, 5 (2019), <https://doi.org/10.17815/jlsrf-5-171>, <http://dx.doi.org/10.17815/jlsrf-5-171>.

[22] X.-L. LIN AND M. K. NG, *An all-at-once preconditioner for evolutionary partial differential equations*. unpublished, 2020, <https://arxiv.org/abs/2002.01108>.

[23] LLBL, *Website for PFASST codes*, 2018, <https://pfasst.lbl.gov/codes>. [Online; accessed July 30, 2018].

[24] LLNL, *XBraid: Parallel multigrid in time*. <http://llnl.gov/casc/xbraid>.

[25] E. McDONALD, *All-at-once solution of time-dependent PDE problems*, PhD thesis, University of Oxford, 2016.

[26] E. McDONALD, J. PESTANA, AND A. WATHEN, *Preconditioning and Iterative Solution of All-at-Once Systems for Evolutionary Partial Differential Equations*, SIAM Journal on Scientific Computing, 40(2) (2018), pp. A1012–A1033, <https://doi.org/10.1137/16M1062016>.

[27] J. NIEVERGELT, *Parallel methods for integrating ordinary differential equations*, Commun. ACM, 7(12) (1964), p. 731–733, <https://doi.org/10.1145/355588.365137>.

[28] B. W. ONG, R. D. HAYNES, AND K. LADD, *Algorithm 965: RIDC Methods: A Family of Parallel Time Integrators*, ACM Trans. Math. Softw., 43 (2016), <https://doi.org/10.1145/2964377>, <https://doi.org/10.1145/2964377>.

[29] B. W. ONG AND J. B. SCHRODER, *Applications of time parallelization*, Computing and Visualization in Science, 23 (2020), <https://doi.org/10.1007/s00791-020-00331-4>, <https://doi.org/10.1007/s00791-020-00331-4>.

[30] D. RUPRECHT, *Wave propagation characteristics of Parareal*, Computing and Visualization in Science, 19(1) (2018), pp. 1–17, <https://doi.org/10.1007/s00791-018-0296-z>.

[31] D. RUPRECHT AND R. KRAUSE, *Explicit parallel-in-time integration of a linear acoustic-advection system*, Computers & Fluids, 59(0) (2012), p. 72–83, <https://doi.org/10.1016/j.compfluid.2012.02.015>.

[32] Y. SAAD AND M. H. SCHULTZ, *GMRES: A Generalized Minimal Residual Algorithm for Solving Nonsymmetric Linear Systems*, SIAM J. Sci. Stat. Comput., 7 (1986), p. 856–869.

[33] R. SCHÖBEL AND R. SPECK, *PFASST-ER: combining the parallel full approximation scheme in space and time with parallelization across the method*, Computing and Visualization in Science, 23 (2020), <https://doi.org/10.1007/s00791-020-00330-5>, <https://doi.org/10.1007/s00791-020-00330-5>.

[34] R. SPECK, *Algorithm 997: pysdc - prototyping spectral deferred corrections*, ACM Transactions on Mathematical Software, 45 (2019), pp. 1–23, <https://doi.org/10.1145/3310410>, <https://doi.org/10.1145/3310410>.

[35] G. A. STAFF AND E. M. RØNQUIST, *Stability of the parareal algorithm*, in Science and Engineering, Lecture Notes in Computational Science and Engineering, e. a. R. Kornhuber, ed., vol. 40, Springer, Berlin, 2005, p. 449–456, https://doi.org/10.1007/3-540-26825-1_46.

[36] J. STEINER, D. RUPRECHT, R. SPECK, AND R. KRAUSE, *Convergence of Parareal for the Navier-Stokes equations depending on the Reynolds number*, in Numerical Mathematics and Advanced Applications - ENUMATH 2013, Lecture Notes in Computational Science and Engineering, A. Abdulle, S. Deparis, D. Kressner, F. Nobile, and M. Picasso, eds., vol. 103, Springer International Publishing, 2015, p. 195–202, https://doi.org/10.1007/978-3-319-10705-9_19.

[37] G. ČAKLOVIĆ, *Paralpha*. <https://github.com/caklovicka/linear-petsc-fft-Paralpha>, 2021.

[38] E. W. WEISSTEIN, *Radau Quadrature*, <https://mathworld.wolfram.com/RadauQuadrature.html>. From MathWorld—A Wolfram Web Resource.

[39] S. L. WU, T. ZHOU, AND Z. ZHOU, *Stability Implies Robust Convergence of a Class of Diagonalization-Based Iterative Algorithms*. unpublished, 2021, <https://arxiv.org/abs/2102.04646>.